Pushed global modes in weakly inhomogeneous subcritical flows

A. Couairon[1], J.-M. Chomaz[2]

[1] *Commissariat à l'Énergie Atomique, Département de Physique Théorique Appliquée, BP 12, F-91680 Bruyères-le-Châtel, FRANCE.*

[2] *Laboratoire d'Hydrodynamique (LadHyX), CNRS UMR 7646, École Polytechnique, F-91128 Palaiseau, FRANCE*

(April 9, 2001)

Abstract

A new type of nonlinear global mode (or fully nonlinear synchronized solution), arising in the dynamics of open shear flows which behave as oscillators [1] and in optical parametric oscillators [2], is identified in the context of the real subcritical Ginzburg–Landau equation with slowly varying coefficients. The nonlinear global modes satisfy a boundary condition accounting for the inlet of the flow. We show that the spatial structure of these new nonlinear global modes consists of a localized state limited by an upstream front that withstand the mean advection and a fast return to zero downstream achieved either by a second stationary front facing backward, or by a saddle node bifurcation driven by the nonparallelism of the flow. We derive scaling laws for the slope of the nonlinear global modes at the inlet and for the position of the maximum amplitude which are in agreement with similar scaling obtained in experiments with a shear layer in a Hele-Shaw cell [3].

PACs: 47.20.-k Hydrodynamic Stability, 47.20.Ky Nonlinearity, 47.54.+r Pattern selection, 47.15.Fe Stability of laminar Flows.

I. INTRODUCTION

Several spatially developing open shear flows such as bluff body wakes or hot jets are now well known to belong to a particular class of flows which behave like oscillators [1]. The relevant mechanism sustaining the oscillations is likely to rely on the existence of a nonlinear self-sustained synchronized structure, the so-called nonlinear global mode, that represents the distribution of the velocity fluctuations tuned at a specific frequency. This mechanism has received growing attention over the last decade since it does not need any feedback loop **to sustain the oscillations.** The association of three physical ingredients is sufficient to obtain a nonlinear global mode: (i) **there is a linearly unstable basic state**; (ii) the geometry is open, i.e., fluid particles enter and leave the experimental domain of interest and the mean advection must be considered; (iii) nonlinearity saturates the linear instability. A right balance between these ingredients has explained the occurrence of self-sustained synchronized structures in parallel open shear flows including convection cells with throughflow or Taylor–Couette flow with crossflow [4–7]. In the astrophysical field, this approach has been also adopted by Tobias *et al.* [8] to investigate similar structures describing the dynamo wave in spherical geometry. The same ideas have been applied to nonparallel open flows [9,10], and to nonlinear dynamo waves riding on a varying background [11,12]. In all these cases, the existence of a nonlinear global mode has been closely related to a linear transition from convective to absolute instability. In the present paper, we consider systems with stronger nonlinearities and show that a new type of nonlinear global mode arise, that does not rely on such a transition.

The notions of absolute and convective instabilities initially developed in the context of plasmas physics [13–15] constitute the association of the first two ingredients and characterize the impulse response of a system with no streamwise variation (parallel flow). If localized disturbances are growing but swept away from the source, the basic state is said to be *convectively unstable*. In other words, the mean advection velocity is sufficiently high in comparison with the growth of perturbations to impose that the amplitude returns back to the basic state at a fixed location. By contrast, if linear disturbances spread and grow upstream and downstream and contaminate the whole medium the basic state is said to be *absolutely unstable*. In the presence of stabilizing nonlinearity, an open flow supports a nonlinear global mode when it is absolutely unstable. In a semi-infinite domain where the origin represents the inlet of the flow, the spatial structure of the global mode is that of a front which withstands the mean advection and is stopped at a finite distance of the inlet (see Fig. 1 below and Refs. [16,17]); this distance is called the growth length of the global mode. In this respect, the problem of front selection has advantageously shed light on the existence conditions of nonlinear global modes in homogeneous systems. In an infinite domain, the interface between a stable nonuniform state and an unstable or metastable homogeneous state constitutes a front propagating into the unstable state at a constant velocity in several experiments [18–20]. The determination of the principles governing the selection of the front velocity as well as the pattern behind the front, its oscillation frequency and the front relaxation has been the topic of active experimental and theoretical research since the early paper by Kolmogorov [21–32]. To be concise, the front propagation may be of two types (pulled or pushed regime) schematically depending on whether the state into which the front propagates is unstable or metastable. A linear (pulled regime) and a nonlinear (pushed regime) marginal stability criterion have been proposed to explain the selection [25,26]. The connection between the front selection problem and the notions of absolute and convective instabilities may be made by rephrasing the linear selection principle: the *pulled* front also referred to as the Kolmogorov front [21,22], is such that, in the frame moving with the front, the basic state is marginally absolutely unstable, i.e., at the threshold between convective and absolute instability. The front is pulled in the sense that its selection among a continuous family, parametrized by its frequency and its velocity, is uniquely determined by the linear properties of the unstable medium in which it propagates. In contrast, the *pushed* front is a faster front that is therefore selected provided it satisfies certain causality conditions [33].

A first type of nonlinear global mode has been shown to exist in semi-infinite domains with a mean advection, when a bifurcation parameter exceeds the ab-

solute instability threshold. These modes therefore rely on the selection of a pulled front stopped in its motion by the upstream boundary. The boundary condition at the inlet breaks the Galilean invariance and slightly distorts the front shape and frequency. The case of homogeneous (parallel) flows achieved only in Taylor–Couette rolls or Rayleigh–Bénard convection with throughflow has been solved [6,7] by determining these distortions from the pulled front. Scaling laws previously obtained [4,5] by numerical integration of Navier–Stokes equations for the growth length of the global modes have been found to agree remarkably well with the analytical scaling laws we derived using the complex Ginzburg–Landau equation (see also the related studies in astrophysics [8]).

Most open flows, however, cannot be considered parallel. **They develop not only in the streamwise direction, but also in the transverse direction** and the effect of inhomogeneity (or nonparallelism) has to be explicitly taken into account. In a previous study [9], we have shown that the real supercritical Ginzburg–Landau equation associated with a weakly varying parameter is surprisingly well suited to describe bluff body wakes, which constitute the archetype of self-resonant open shear flows. Indeed, the spatial structure of numerically [34] or experimentally [35] measured wakes has been found to be in accordance with the analytically derived structure of the nonlinear global modes of our model, which still possess the shape of a pulled front, but the saturated part of the solution smoothly returns to zero in the tail. **Borrowing the front terminology, these nonlinear global modes will be referred to as "pulled global modes".** We have derived scaling laws for the maximum amplitude of the pulled global modes and its position which compare satisfactorily with those found experimentally by Goujon-Durand et al. [35] or numerically by Zielinska & Wesfreid [34]. Similar nonlinear global modes have been identified for optical parametric oscillators [36] and in amplitude evolution models of solar and stellar magnetic activity cycles [11,37]. There is an extensive literature on these structures in the astrophysical context for which the reader is referred to Ref. [12] and Refs. therein for a review. **A locally absolutely unstable region in the flow is necessary to trigger the nonlinear global instability and the emergence of a pulled global mode.** The latter scenario shown in Ref. [9] for semi-infinite domains was already valid for the occurrence of a self-sustained linear global mode [38] and is still valid for the emergence of pulled global modes in an infinite domain governed by the supercritical Ginzburg–Landau equation with varying coefficients, thoroughly studied by Pier *et al.* [10].

As expected from the front selection problem, however, a second type of nonlinear global mode exists, the spatial structure of which is associated with an upstream front belonging to the class of pushed fronts and separating the inlet from the saturated amplitude. Still borrowing the front terminology, these modes will be called "pushed global modes". In homogeneous fully nonlinear systems, addition of a generic nonlinearity such as a weak subcritical effect or nonlinear advection promotes the emergence of pushed global modes [16,17,39]. In this case, the medium does not need to be absolutely unstable; nonlinear absolute instability in the sense of Chomaz [40] is sufficient. The recent experiments by Gondret *et al.* [3] for a Kelvin-Helmholtz sheared interface in a Hele-Shaw cell have shown experimental evidence, for the first time in a fluid system, of a nonlinear transition from convective to absolute instability through a weak subcriticality. In this experiment, the healing length, defined as the distance from the inlet necessary to reach saturation, has been measured and shown to scale logarithmically as a function of the departure from threshold, in agreement with the scaling obtained theoretically in Refs. [16,17].

The objective of the present paper is to describe the pushed global modes in nonparallel open shear flows where nonlinearity is destabilizing. The identification of these self-synchronized structures is now timely. We address the question of their existence and scalings in nonparallel subcritical systems. The rising part of the pushed global modes is steeper than that of the pulled global modes [9], as will be shown by the particular scaling laws for the slope and the position of the maximum amplitude. Moreover, the pushed global modes do not exhibit a smooth tail as the pulled modes obtained in supercritical systems [9]; instead, a second front facing backward is present downstream with amplitude decreasing back to zero. The existence of pushed global modes in optical parametric oscillators has been shown numerically very recently [2]. In open shear flows, these modes are likely to arise in subcritically unstable systems such as Poiseuille or Couette flow in a slow diverging pipe, Görtler flow or wakes confined in a channel. Gondret *et al.*'s experiment performed in a slowly diverging

Hele-Shaw cell could constitute a particular setup suited to test the emergence and scalings of these modes.

The outline of the paper is as follows: In section II, we present our real Ginzburg–Landau model which is not rationally derived from fluid equations describing the dynamics of a particular open flow, but is to be seen as an idealized model with the necessary physical ingredients to describe the self sustained oscillations. In section III, we will present qualitatively the spatial structure of the pushed global modes obtained for this model. In section IV, scaling laws for the slope and the position of the maximum amplitude of the nonlinear global modes are explicitly derived. **Numerical simulations are presented in section V and show that pushed global modes persists when our model is extended to the case of the complex Ginzburg–Landau equation.** Finally, Section VI is devoted to the discussion of results and conclusion.

II. THE SUBCRITICAL GINZBURG–LANDAU MODEL

We will consider a toy model that possesses all the necessary physical ingredients to mimic the behavior of an open subcritical shear flow such as the Poiseuille flow, with an upstream boundary from which perturbations develop. Moreover, the flow is allowed to evolve slowly in space. The nonlinear self-sustained oscillations, or nonlinear global modes, that such a flow display under certain conditions are usually tuned at a well defined frequency. In the present paper, we will first focus on the spatial structure of these modes. **We will then briefly go back to the frequency selection problem in section V where we will show how the results extend in the oscillatory case**. Our toy model is therefore constituted by the real subcritical Ginzburg–Landau equation with a positive advection velocity U_0 which models the mean flow, and a slowly varying coefficient $\mu(x)$:

$$\frac{\partial A}{\partial t} + U_0 \frac{\partial A}{\partial x} = \frac{\partial^2 A}{\partial x^2} + \mu(x)A + A^3 - A^5. \tag{1}$$

We will present the spatial structure of nonlinear global (NG) modes which are steady solutions of (1) in a semi-infinite domain representing the region in which the flow develops, and satisfying the ideal inlet condition

$$A(x=0)=0, \tag{2}$$

accounting for a zero level perturbation. The second boundary condition is the asymptotic behavior at $x=+\infty$ dictated by the fact that the system is assumed here to be sufficiently stable at infinity. We therefore consider only solutions asymptotic to 0 when $x=+\infty$ (*i.e.* such that $\mu(+\infty)<-1/4$).

$$A(+\infty)=0. \tag{3}$$

The latter condition may easily be relaxed: for example if the bifurcation parameter is asymptotic to a constant at infinity ($\mu(+\infty)=\mathrm{Cst}$), this condition would be that A reach at infinity a minimum of the potential from which terms of the right hand side of Eq. (1) derive (*i.e.* $V(A)=\mu A^2/2+A^4/4-A^6/6$). In the same manner, only the local bifurcation parameter $\mu(x)$ varies in space in our model because this assumption is sufficient to obtain the spatial structure of NG modes; however our analysis applies when each coefficient in front of the terms of Eq. (1) varies.

In order to give a concrete example, the bifurcation parameter is assumed to depend linearly on the space variable x

$$\mu(x)=\mu_0-\mu_1 x \tag{4}$$

where μ_0 and μ_1 are positive constants. Therefore, the system is similar to the one used in [38,9] but with a subcritical nonlinear potential. The choice of a linear dependence in Eq. (4) does not restrict the generality of the study which remains valid as long as $\mu(x)$ is any slowly decreasing function depending on x only through a slow space variable $X=x/L$; (L measures the inhomogeneity length scale and is equal to μ_1^{-1} in the present case). Since the spatial structure of the NG modes strongly relies on the results found in the constant μ case, we begin with a brief summary of the latter results.

A. Constant μ case

The constant μ case models parallel open flows, i.e., flows where the velocity profile constituting the basic state does not vary in the direction transverse to

the flow. In the parallel flow case ($\mu_1 = 0$ and $\mu = \mu_0$), we have determined in [17], for the same subcritical Ginzburg–Landau model, the transition to a global instability and the associated spatial structure of steady solutions of Eq. (1) vanishing at the origin and saturating at a finite amplitude when $x \to +\infty$. When the bifurcation parameter does not vary with respect to x, in order to avoid confusion, these solutions will be denoted "homogeneous" nonlinear global (HNG) modes throughout the study. In this case, a NG mode satisfies at $x = 0$ the boundary condition (2) and at infinity, Eq. (3) is replaced by: $A(+\infty) = A_2(\mu_0)$ with

$$A_2(\mu) = \left(\frac{1}{2} + \sqrt{\mu + 1/4}\right)^{\frac{1}{2}}. \tag{5}$$

Figure 1 shows the spatial structure of such a HNG mode constituted by a front halted in its upstream motion by the boundary condition and separating the inlet at $x = 0$ from the saturated region.

FIG. 1

HNG modes exist in the shaded region (Fig. 2) of parameter space (U_0, μ) limited by $\mu > \mu_A(U_0)$ with

$$\mu_A(U_0) = \frac{3}{16}U_0^2 + \frac{\sqrt{3}}{8}U_0 - \frac{3}{16} \quad \text{if} \quad U_0 < \sqrt{3} \tag{6}$$

$$\mu_A(U_0) = \frac{U_0^2}{4} \quad \text{if} \quad U_0 > \sqrt{3} \tag{7}$$

In [17], depending on whether (6) or (7) holds, we have characterized the conditions of emergence of these HNG modes and we have determined two different scaling laws for their growth length Δx, versus the **departure from global instability threshold**

$$\epsilon = \mu - \mu_A. \tag{8}$$

The quantity Δx is defined as the distance at which the solution reaches 50% of its maximum amplitude A_2.

FIG. 2

- When $U_0 > \sqrt{3}$, the threshold for the existence of a global mode does correspond to the change in the linear instability of the basic solution $A = 0$ from convective to absolute. HNG modes exist only when small amplitude waves are absolutely unstable (dark gray region of Fig. 2 limited by $\mu = U_0^2/4$). In this case, the transition has been called of Kolmogorov type since it corresponds to a Kolmogorov front [21] blocked on the origin. The growth length Δx scales as

$$\Delta x = \frac{\beta}{\sqrt{\epsilon}} \quad \text{(Kolmogorov K type)}, \tag{9}$$

where $\beta = \pi$ for Equation (1). A similar scaling in $\epsilon^{-1/2}$ has been found for the growth length of HNG modes obtained for the supercritical real or complex Ginzburg–Landau model [16,17], for which the transition to global instability is always of the Kolmogorov type. **Although the quantity $\epsilon^{-1/2}$ is the natural Ginzburg–Landau length scale, the coefficient β is obtained exactly by non trivial matched asymptotic expansions.** This scaling has been experimentally and numerically verified for Rayleigh–Bénard convection with throughflow and Taylor–Couette experiments with throughflow [6,7].

- When $U_0 < \sqrt{3}$, the threshold of existence (6) of a HNG mode is not linked to a change in the nature of the linear wave instability, but from nonlinear effects that are able to withstand the advection. Therefore, the global modes obtained in that case have been called of nonlinear type (following a classical differentiation made for front solutions [22]). HNG modes exist while the system is convectively unstable or stable (light gray region of Fig. 2). For fixed U_0, when increasing μ, the global instability occurs before the absolute/convective transition (it is therefore called "nonlinear transition") and the HNG modes are much steeper than in the previous case with a growth length scaling as $\log(1/\epsilon)$:

$$\Delta x \simeq \log(\frac{1}{\epsilon}) \quad \text{(Nonlinear N type)}. \tag{10}$$

This scaling has very recently been observed for a Kelvin–Helmholtz sheared interface in a Hele–Shaw cell [3]

B. Varying μ case

In the varying μ case ($\mu_1 \neq 0$ or nonparallel flow case), we will restrict our presentation to the range $0 \leq U_0 < \sqrt{3}$ in which a nonlinear transition of the parallel flow to global instability occurs. For $U_0 > \sqrt{3}$, the Kolmogorov transition occurs and the structure and the final results are nearly identical to those obtained for the supercritical model presented in [9]. Only the downstream part of the structure is different: instead of a smooth return to zero, it is constituted by a sharp return to zero similar to that obtained in the structure for $1/\sqrt{3} < U_0 < \sqrt{3}$, which will be described below.

At the origin of the semi-infinite domain, we assume that the bifurcation parameter μ_0 is larger than the NG instability threshold *i.e.* the threshold $\mu_A(U_0)$ (Eq. 6) of emergence of HNG modes:

$$\mu_0 = \mu_A + \epsilon. \tag{11}$$

If ϵ is sufficiently large, a NG mode may grow in space and saturate before the local bifurcation parameter $\mu(x)$ has become smaller than $\mu_A(U_0)$, whose dependence in U_0 will no longer be mentioned for the sake of clarity. Therefore, we will not only use a weakly nonparallel hypothesis ($\mu_1 \ll 1$), but also a stronger condition ensuring that nonlinearity "dominates" over nonparallelism in a sense that we will precise. As in [9], we face here a singular perturbation problem as the two limits $\mu_1 \to 0$ and $\epsilon \to 0$ cannot be taken at the same time and respective orders have to be specified (nonuniform limit). The physical guideline for the ordering in small parameters relies on comparing the typical length scales associated with nonlinearity (departure from threshold ϵ) quantified by Δx and the length scale of the inhomogeneity characterized by the distance x_A from the origin at which $\mu(x_A) = \mu_A$. Let us also introduce x_s, the position of the maximum amplitude of the NG mode. When the growth length Δx of HNG modes is sufficiently small in comparison with the inhomogeneity length scale $\Delta x \ll x_A$, we can describe the spatial growing part of the NG mode as the leading edge of the corresponding HNG mode (with the constant parameters $\mu = \mu_0$ and U_0) and write $x_s \sim \Delta x \sim \log(1/\epsilon)$. Using formula (10) for the growth length of HNG modes, the hypothesis that $\Delta x \ll x_A$ gives:

$$\Delta x \ll \frac{\epsilon}{\mu_1} \Rightarrow \mu_1 \ll \frac{\epsilon}{\log(1/\epsilon)} \tag{12}$$

Under this hypothesis, we may describe the spatial structure of a NG mode of Eq. (1), rigorously defined as a solution of the equation

$$\frac{d^2A}{dx^2} - U_0\frac{dA}{dx} + (\mu_0 - \mu_1 x)A + A^3 - A^5 = 0, \tag{13}$$

vanishing at $x = 0$ and $x \to +\infty$, by interpreting its growing part as the leading edge of a HNG mode and its decreasing part as the adiabatic variation of the saturation amplitude $A_2(\mu)$ with respect to x through $\mu(x)$. As will be seen below, in some cases, **the NG mode follows adiabatically $A_2(\mu(x))$ over a finite length only, and then decreases faster in space than $A_2(\mu(x))$. This does not** alter the first steps of our analysis and modifies only the trail of the NG modes.

At this stage, we must anticipate on the result which will be found for x_s in order to set correctly the condition of validity of the analysis, which turns out to be slightly different from (12): x_s will be found to possess a dominant contribution which scales as $\log(1/\mu_1)$, and therefore exceeds the expected contribution $\log(1/\epsilon)$ coming from Δx (as if the NG mode was homogeneous). The condition $x_s \ll x_A$ is more restrictive than $\Delta x \ll x_A$ and then reads

$$\frac{\epsilon}{\mu_1} \gg \log\frac{1}{\mu_1} \tag{14}$$

Our goal is to describe the spatial structure of NG modes when condition (14) is satisfied. In particular, we seek a scaling law for the position x_s of the maximum amplitude. Let us emphasize that x_s is expected to be at least greater than the growth length of HNG modes $\log(1/\epsilon)$.

III. SPATIAL STRUCTURE OF PUSHED GLOBAL MODES

FIG. 3

A generic example of the ultimate state, i.e., a pushed global mode obtained in a temporal numerical simulation of Eq. (1), with vanishing boundary conditions at the origin and at infinity, is displayed in Fig. 3. Initially the system is set in the uniform state $A = 0$. **When the advection velocity is in the range $[1/\sqrt{3}, \sqrt{3}]$, Eqs. (4), (6) and (11) show that $\mu_A(U_0) > \mu_A(1/\sqrt{3}) = 0$ and $\mu(x) > 0$ near the origin. Thus the medium is linearly**

unstable in a region of finite extent beyond $x = 0$. Due to infinitely small perturbations, the amplitude grows and asymptotes a steady state such as that displayed in Fig. 3. When the advection velocity is smaller than $1/\sqrt{3}$, the medium is stable near the origin, but finite amplitude perturbations are able to destabilize the system which eventually converges to a steady state of similar spatial structure. The spatial structure of the NG mode will be described in the general case by using the method of matched asymptotic expansions [41]. We distinguish seven subdomains in the original semi-infinite domain represented in Fig. 3.

The nonlinear front layers NF^s (saturated), NF^d (downstream), the central nonlinear layer CNL and a linear outer layer OL are separated by transition layers (inner layers), namely, IL at the origin, TL^s around x_s the location of the maximum amplitude, TL^d around the point x_d which represents the right boundary of CNL and will be specified below. The respective sizes of the layers are indicated on Fig. 3. In the following, we indicate only briefly the nature of the solutions in each layers. The size of the different layers may be obtained only by the matching, the mathematical details of which are postponed in Appendix A.

A. Qualitative description of pushed global modes

In each subdomain, we must solve Eq. (13) and we need two boundary conditions in order to find the corresponding solution. Since we only know the boundary conditions at the origin and at infinity of the whole domain, the matching between the different layers we have introduced will determine all integration constants.

1 - *Inner layer* IL of size $\mathcal{O}(\log \epsilon^{-1})$: since the amplitude remains small, we use a solution of Eq. (13) linearized around zero, and the two integration constants are fixed by the boundary condition at the origin and the matching, detailed below, with the solution in NF^s.

2 - *Nonlinear front layer* NF^s of size $\mathcal{O}(1)$: the solution is similar to the homogeneous global mode which grows in space till it reaches its maximum amplitude (Fig. 1) with an added small perturbation due to inhomogeneity. Since this solution is **growing on an order one length scale**, the bifurcation parameter can be considered as a constant [which

equals $\mu_A(U_0)$, Eq. (6)] at leading order. We use the study of the parallel model Eq. (13) with $\mu_0 = \mu_A(U_0)$ to find the corresponding solution and compute the correction due to inhomogeneity.

At x_s, the bifurcation parameter is close to the value $\mu_A(U_0)$ when neglecting ϵ and $\mu_1 \log \epsilon$ terms. The matching between NF^s and TL^s is used as a boundary condition for the solution in NF^s. For this reason, the solution in NF^s can be computed unambiguously, only after the solution in TL^s is worked out.

3 - *Transition layer* TL_s of size $\mathcal{O}(\log \mu_1^{-1})$: the amplitude has to match with the solution in NF^s and therefore is close to $A_2(\mu_A)$ [Eq.(5)]. It is represented by a solution of Eq. (13) linearized around $A_2(\mu_A)$. The matching with CNL on the one hand, and the condition that $A(x)$ realizes a maximum at x_s on the other hand determine the two integration constants. Again, the solution in TL^s can be only determined after the solution in CNL, the next layer downstream, is known.

4 - *Central nonlinear layer* CNL of size $\mathcal{O}(\mu_1^{-1})$: it denotes the subdomain where the solution has bifurcated to the finite amplitude state $A_2(\mu)$ [Eq.(5)] and follows adiabatically the weak variation of the bifurcation parameter $\mu(x)$. The pushed global mode amplitude decreases slowly from $A_2[\mu(x_s)]$ to $A_2[\mu(x_d)]$, following approximately the slowly varying function $A_2[\mu(x)] = [1/2 + \sqrt{\mu_0 - \mu_1 x + 1/4}]^{1/2}$ and reflecting the interplay between nonlinearities and inhomogeneity. CNL boundaries x_s and x_d actually determine the locations where the slope of the solution starts to steepen (with growing or decreasing amplitude). The left boundary x_s has been already defined as the position of the maximum amplitude, but the right boundary x_d which is the position of the decreasing front will be specified below.

5 - *Transition layer* TL^d of size $\mathcal{O}(\log \mu_1^{-1})$ around x_d: it plays the same role as TL^s with $A_2(\mu_A)$ replaced by $A_d = A_2(\mu_d)$, $\mu_d = \mu(x_d)$ and the condition that $A(x)$ be maximum at x_s is replaced by the condition that $A(x)$ exactly be equal to A_d at x_d.

6 - *Nonlinear front layer* NF^d of size $\mathcal{O}(1)$: the solution decreases back to a small amplitude **on an order one length scale** and we again consider that this decreasing solution is a stationary backward facing nonlinear front with corrections due to inhomogeneity.

The position x_d of the decreasing front linking the finite amplitude state to zero is determined by considering the existence of the front in the homogeneous problem where the bifurcated state relaxes back to zero. **For $U_0 > 1/\sqrt{3}$, this occurs through a saddle node bifurcation, i.e., the saturated state $A_2(\mu(x))$ loses its existence at a finite amplitude when μ decreases and reaches the value**

$$\mu_d(U_0) = -\frac{1}{4} \quad \textbf{if} \quad U_0 > \frac{1}{\sqrt{3}}. \tag{15}$$

For $U_0 < 1/\sqrt{3}$, this occurs when the bifurcation parameter reaches a larger value $\mu_d(U_0)$ such that an heteroclinic orbit [which represents the steady front solution in the phase space $(A, dA/dx)$] connects $(A_2(\mu_d), 0)$ to the origin $(0, 0)$. In other words, for $\mu = \mu_d(U_0)$, the stable manifold of the origin of phase space intersects the unstable manifold of the fixed point $(A_2(\mu_d), 0)$. In a previous study [17], we have determined the decreasing front transition value $\mu = \mu_d(U_0)$ which is plotted in Fig. 2 with a fine line and has parametric equation

$$\mu_d(U_0) = \frac{3}{16}U_0^2 - \frac{\sqrt{3}}{8}U_0 - \frac{3}{16} \quad \text{if} \quad U_0 < \frac{1}{\sqrt{3}} \tag{16}$$

Returning to the inhomogeneous problem, the position of the decreasing front is determined by $\mu(x_d) = \mu_d$.

FIG. 4

Let us point out that the whole structure of the pushed global mode has been pinned by the position of CNL between x_s and x_d. Actually, Fig. 3 may be viewed as the projection in the (A, x) plane of the three-dimensional phase space $(A, dA/dx, x)$. Fig. 4 shows the structure of the solution in the phase space: the growing and decreasing fronts in NF^s and NF^d lay nearly in planes parallel to $(A, dA/dx)$ and correspond to rapid variations of A with $\mu(x)$ nearly frozen, whereas the solution in CNL follows adiabatically the variation of $\mu(x)$ and lays nearly in the (A, x) plane. From the left and right boundaries x_s and x_d of the central nonlinear layer CNL, now precisely known from the variation of $\mu(x)$, we obtain that the size of CNL is $\mathcal{O}(\mu_1^{-1})$, since $x_d \sim \mu_1^{-1} \times [\mu_A(U_0) - \mu_d(U_0)]$ and $x_s \ll \mu_1^{-1}$. The whole solution is therefore pinned by CNL since the matching can be performed from CNL to the nonlinear front layers: solutions in NF^s and NF^d can be computed by applying only one boundary condition given by the matching with CNL via TL^s and TL^d. However, the whole matching must be done in order to verify that the boundary conditions (2) and (3) can be indeed satisfied and to know precisely the restrictions on μ_1 and ϵ these boundary conditions imply. Nevertheless, this constitutes the last stage of the matching and does not alter the spatial structure of the solution described above.

7 - *Outer layer* OL: the solution must vanish at infinity and hence, the amplitude remains small. We therefore use a solution of Eq. (13) linearized around zero, and fix the remaining integration constant and the order of magnitude of the amplitude in OL by the matching with NF^d. The matching of the trail in OL is always possible and does not require an extra transition layer since the trail is slaved to the upstream structure of the NG mode.

The complete spatial structure of NG modes represented on Fig. 3 for model (13) is detailed for each layer in Appendix A. Only the matching between the inner layer IL and the front layer NF^s is detailed in the next section since it determines the scaling law for the position x_s of the maximum amplitude of the NG mode.

IV. MATCHING $IL \to NF^S$ AND SCALING LAW FOR THE POSITION OF THE MAXIMUM

The inner solution in IL and the outer solution in NF^s are obtained in Appendix A. Denoting by ξ the inner variable for the amplitude in IL, the matching between these layers is done in a plane $(A, dA/dx)$ (Fig. 4), i.e. we match dA/dx [considered as a function of A] when $A \to 0$, with $d\xi/dx$ when $x \to +\infty$. When $x \to +\infty$, the asymptotic behavior of the inner solution (A32), i.e., $d\xi/dx$ as a function of ξ reads as

$$\frac{d\xi}{dx} \simeq r^+\xi + v_0^{1-r^-/r^+} \left(r^+ - r^-\right)^{r^-/r^+-1} \xi^{r^-/r^+} \tag{17}$$

where $r^+ = (U_0 + \sqrt{3})/4$ and $r^- = (3U_0 - \sqrt{3})/4$. The quantities r^+ and r^- represent the spatial exponential growth (or decay) rates linked to possible ways to depart from (or arrive to) zero. The quantity v_0 represents the slope at the origin of the inner solution (and will be given by the matching). Multiplication of Eq. (17) by $\theta(\epsilon)$ (where $\theta(\epsilon) \to 0$ is the size in amplitude of the inner layer and will be specified below) and introduction of $A = \theta(\epsilon)\xi$ in

Eq. (17) yields the following expansion (inner solution rewritten in outer variable)

$$\theta(\epsilon)\frac{d\xi}{dx} \simeq \frac{A_s^2}{\sqrt{3}}A + [v_0\theta(\epsilon)]^{1-\lambda_1}\left(r^+ - r^-\right)^{\lambda_1} A^{\lambda_1}, \tag{18}$$

where $A_s \equiv A_2(\mu_A)$ and $\lambda_1 = r^-/r^+$. The asymptotic behavior of the solution $u(A) \equiv dA/dx(A)$ in NF^s when $A \to 0$ is given by Eq. (A30) of Appendix A. For the matching, we note that $r^+ = A_s^2/\sqrt{3}$. Equation (18) must be compared with expansion (A30) in NF^s. The zeroth order terms are identical. At next order, we must identify $\theta(\epsilon)^{1-\lambda_1}$ with either ϵ or $\mu_1 \log(1/\mu_1)$. When $\mu_1 \log(1/\mu_1) \ll \epsilon$, ϵ is the dominant term in (A30) and the matching of solution (18) with solution (A30) in NF^s yields

$$\theta(\epsilon) = \epsilon^\beta, \qquad \text{with} \qquad \beta = \frac{1}{1-\lambda_1}, \tag{19}$$

and

$$v_0 = \left(\frac{\sqrt{3}A_s^{2\lambda_2}}{(r^+ - r^-)^{\lambda_1}} \int_0^{A_s} a^{-\lambda_1}(A_s^2 - a^2)^{-\lambda_2 - 1} da\right)^\beta, \tag{20}$$

λ_2 being given by Eq. (A27) of Appendix A. The position of the maximum is given by the sum of the contribution in IL found by Eq. (A33) from $x = 0$ to x_i where $\xi = 1$:

$$x_i \simeq \frac{1}{r^+} \log \frac{r^+ - r^-}{v_0}, \tag{21}$$

and the contribution in NF^s and TL^s found by Eq. (A25) from x_i where $A = \theta(\epsilon)$ to x_s:

$$x_s - x_i \simeq \frac{1}{k_s^-}(2\beta \log \epsilon + \log \mu_1). \tag{22}$$

where $k_s^- = -2A_s^2/\sqrt{3}$. From the condition $\mu_1 \log(1/\mu_1) \ll \epsilon \ll 1$, we obtain $\log(1/\epsilon) \ll \log(1/\mu_1)$. Therefore, when keeping only the dominant term in x_s, we find

$$x_s \simeq \frac{1}{|k_s^-|} \log\left(\frac{1}{\mu_1}\right) \tag{23}$$

Our analysis is therefore valid for $\epsilon \gg \mu_1 \log(1/\mu_1)$ and the dominant contribution to the position of the maximum x_s is given by (23), i.e., it scales as $\log(1/\mu_1)$. This result differs from the one found for pulled global modes for which the location x_s of their maximum amplitude has been found to scale as $1/\sqrt{\epsilon}$, as for the growth length of their homogeneous counterpart.

The dominant part $\log(1/\mu_1)$ of the scaling law for x_s has been shown to exceed the growth length of homogeneous NG modes which scales as $\log(1/\epsilon)$. This difference comes from the fact that a homogeneous NG mode never reaches a maximum but asymptotes it at $+\infty$. Its growth length is mainly given by the distance from the inlet necessary to grow out of the inner layer. In contrast, a NG mode not only grow out of the inner layer over the same distance, but also needs an extra length which is $\mathcal{O}[\log(1/\mu_1)]$ to reach its maximum amplitude. Since our analysis is valid when both parameters ϵ and μ_1 go to zero, with the condition $\epsilon \gg \mu_1 \log(1/\mu_1)$, the dominant contribution in the position of the maximum of the NG mode is constituted by this extra length.

V. NUMERICAL SIMULATIONS IN THE OSCILLATORY CASE AND FREQUENCY SELECTION PROBLEM

In physical systems where the instability is oscillatory, the Ginzburg–Landau model (1) studied in the previous sections must be extended to the case where all coefficients are complex and vary with x. We will show numerically that the spatial structure of the pushed global modes found in the framework of the real equation (1) persists for the complex case which reads:

$$\frac{\partial A}{\partial t} + U_0 \frac{\partial A}{\partial x} = (1 + ic_1)\frac{\partial^2 A}{\partial x^2} + \mu A + (1 + ic_3)|A|^2 A - (1 - ic_5)|A|^4 A. \tag{24}$$

Since the results obviously extend to the case when all coefficients vary, we will consider that only the bifurcation parameter μ and the advection velocity U_0 vary with x, while other coefficients including c_1, c_3, c_5 and those set to unity are kept constant.

Numerical simulations of Eq. (24) have been performed with the initial condition $A(x, t = 0) = 0.8$ for $3 < x < 50$ and $A(x, t = 0) = 0$ otherwise. When the state $A = 0$, referred to as the medium, is stable, this localized initial condition of finite amplitude is necessary to trigger the evolution to an ultimate state, either oscillatory in the form of a pushed global mode or exhibiting a more disordered behavior. When the medium is unstable, an infinitesimal initial condition is sufficient to obtain the same result. In any case, the final state of the system

is not very sensitive to the initial condition, provided the latter is sufficiently localized.

Figure 5 shows the amplitude and real part of the pushed global mode obtained for the set of parameters close to the real case: $U_0 = 0.02$, $\mu(x) = (1+0.1i)\times(-0.05-10^{-3}x)$, $c_1 = c_3 = c_5 = 0$. The asymptotic state is a pushed mode such as that described in the previous sections, with an upstream front stopped at the inlet, a saturated amplitude following the variation of parameters and a downstream front. The position of this dowstream front at $x_d = 170$ coincides with that marked by the small tick on the axis in Fig. 5(a) which is given by the condition $Re(\mu(x_d)) = \mu_d(U_0)$, where μ_d is given by Eq (16). In this case, the saddle node bifurcation is found when $\mu(x) = -1/4$ and is located at $x = 200$, where the solution has already returned to zero. In Fig. 5(b), another pushed global mode is shown. It has been obtained asymptotically for long times for the parameters $U_0 = 0.6$, $\mu(x) = 0.05 - 10^{-3}x$, $c_1 = 0.1$, $c_3 = 0.3$, $c_5 = -0.1$. The departure from threshold $\epsilon = \mu_0 - \mu_A = 7.3\times10^{-3}$ is comparable to the inhomogeneity parameter $\mu_1 = 10^{-3}$. The position of the upstream front is therefore very close to the point marked by the tick at $x = 7.32$ on the axis where $\mu(x) = \mu_A(U_0)$. In contrast with the pushed global modes in Fig. 5(a) where a decreasing front constituted the tail of the solution, the amplitude in Fig. 5(b) returns to zero due to the saddle-node bifurcation induced by the variation of the parameters. The second tick at $x = 300$ marks its position beyond which the saturated amplitude no longer exists as $\mu(x) < -1/4$. This does not make a great difference in the shape of the tails except for the location of the abrupt decrease, precisely predicted by either the loss of existence of the saturated solution or the existence of a second decreasing front matching the solution before the saddle-node bifurcation occurs.

When such a pushed global mode is obtained, it oscillates globally at a well defined frequency. This frequency imposed at the whole solution is that of the upstream front which acts as the frequency generator for the entire medium. We have measured numerically the frequency of the pushed global mode obtained in

Fig. 5(b). This has been done by averaging a sufficiently large number of cycles when the amplitude seems to have reached a steady state. We have obtained $\omega = -0.1207$; this must be compared to the theoretical value for the pushed front frequency $\omega^\dagger = -0.1151$ obtained from Eq. (3.39c) in [26]. Since the departure from threshold is small, the agreement between the pushed front frequency and the pushed global mode frequency is here excellent. For comparison with these values, the frequency of the nonselected pulled front given by Equation (4.8c) in [26] is $\omega^* = -8.911 \times 10^{-3}$. For larger departures from threshold, the presence of the boundary slightly distorts the frequency of the pushed front. A phase space analysis presented in [7] in the case of pulled global modes allows us, however, to compute these distortions exactly.

Due to the variation of the parameters, more complicated situations may arise: a pushed global mode is not systematically selected by the dynamics in Eq. (24). We will present two cases where a more disordered solution appears.

(i) The saturated amplitude that a pushed global mode follows adiabatically between the upstream and the downstream front may become unstable. In this case, numerical simulations show that the upstream part of a pushed global mode, including the front blocked on the boundary and a part of the saturated tail, is obtained asymptotically for long times; the tail, however, cannot follow the adiabatic variation of the parameters and loses stability. Fig. 5(c) shows that the solution does not converge to an oscillating mode with a single frequency. For this solution the parameters are $U_0 = 0.6 - 0.1 \times [1 + \tanh(0.02x - 3)]$, $\mu(x) = 0.09 - 6 \times 10^{-4} x[1 + \tanh(0.02x - 5)]$, $c_1 = 0.1$, $c_3 = 0.3$ and $c_5 = -1$. The variation of the advection velocity and the bifurcation parameter are shown in Fig. 5(d). They have been specifically chosen such that the slowly varying saturated wave at the frequency imposed by the upstream front loses its stability. A more chaotic dynamics is obtained in the tail where a secondary bifurcation seems to have occurred.

(ii) We have already mentioned that in the real case, for $U_0 > \sqrt{3}$, the nonlinear global modes obtained asymptotically for long times are not pushed global

modes but pulled global modes similar to those described in [9]. They exhibit a pulled upstream front acting as the frequency generator for the whole medium, and a smooth tail. Similar situations arise for Eq. (24): above a certain velocity threshold, the pushed global modes do not exist. Pulled global modes arise as long time asymptotic solutions when imaginary parts of the coefficients in Eq. (24) are not too large. More complicated situations may happen, however, for large values of c_1, c_3 or c_5. In Fig. 5(e), it is shown that for the parameters are $U_0 = 0.2$, $\mu(x) = 0.32 - 8 \times 10^{-4} x$, $c_1 = 1$, $c_3 = 0.3$ and $c_5 = 0.4$, neither a pushed global mode, nor a pulled global mode, nor even an oscillatory state is eventually obtained for long times. This may seem surprising since the criteria for the front selection problem predict the selection of a pulled front. In this case, the advection velocity is imposed and we do not face with a selection problem but an existence problem. Pulses are recurrently nucleated from the region of absolute instability bounded by the origin and the first tick on the axis, and then travel along the convective and stable region, beyond the second tick. This behavior is very similar to what is observed in the Gondret *et al.* experiment [3].

The pushed global modes are therefore relevant to the dynamics provided: (i) the pushed front exists and (ii) the slowly varying saturated plane wave is stable or at least convectively unstable in the entire medium.

VI. DISCUSSION OF RESULTS AND CONCLUSION

A complete description of self-synchronized structures in a semi-infinite open flow is now achieved with the identification of the new structure, called pushed global mode, derived from the model of the present paper. In the following, we briefly recall our results and the different open shear flows to which each nonlinear global mode pertains.

In the parallel flow case, the nonlinear global instability may be either of the Kolmogorov type, i.e., occurring when the **basic state** becomes absolutely unstable, or of the nonlinear type, i.e., occurring while the **basic state** is still convectively unstable. Whether the advection velocity is small or large distinguishes both situations; however, the nonlinear transition does not necessarily occur for small advection velocities. Nor is it restricted to subcritical systems. Addition of nonlinear advection terms in a supercritical model ("van der Pol–Duffing" system in reference [17]) indeed leads to a nonlinear transition for large advection velocities. In the case of a Kolmogorov transition, the growth length of homogeneous nonlinear global modes has been shown [17] to scale as $\epsilon^{-1/2}$, where ϵ is the departure from threshold. In the case of a nonlinear transition, the growth length of homogeneous nonlinear global modes scales as $\log(1/\epsilon)$.

In the weakly nonparallel flow case, the nonlinear global instability may also be of both types. In the case of the Kolmogorov transition, pulled global modes are obtained when a sufficiently large domain of absolute instability in the **medium** triggers the global instability. The position of their maximum amplitude scales as $\epsilon^{-1/2}$. For the model of the present paper, these pulled modes are obtained for large advection velocities ($U_0 > \sqrt{3}$). They are also relevant to describe wakes when inhomogeneity is sufficiently weak as shown in [9]. In the case of the nonlinear transition, pushed global modes are obtained above the threshold of global instability, which is triggered even if no absolute instability region is present in the **medium**. The position of the maximum amplitude of the pushed global modes scales as $\log(1/\mu_1)$ and, to our knowledge, this scaling has not been observed experimentally in a weakly nonparallel flow.

A $\log(1/\epsilon)$ scaling has been obtained in the parallel flow case for the growth length in the Kelvin–Helmholtz unstable interface in a Hele–Shaw cell, by Gondret *et al.* [3]. The $\log(1/\mu_1)$ scaling could be obtained in a similar experiment by addition of a weak inhomogeneity. We conclude this paper by emphasizing that, although the $\log(1/\mu_1)$ scaling is not specific to subcritical systems, an experiment known to display a subcritical behavior (which could be achieved by adding a Poiseuille flow) may lead to the observation of the latter scaling. Görtler flow seems to us a good candidate where these scalings for the pushed global modes could be observed. In optical parametric oscillators [2], pushed global modes with the spatial structure of the present paper have been already identified; hence, the latter system is also well suited to test the scaling laws of the present paper.

APPENDIX A: DETAILED SPATIAL STRUCTURE OF PUSHED GLOBAL MODES

Since the spatial structure of the solution is similar in NF^s and NF^d, and also in TL^s and TL^d, we will use the following notations throughout the appendices to avoid the double description of the layers.

$$\mu_s \equiv \mu_A, \quad A_s \equiv A_2(\mu_A), \tag{A1}$$

$$A_d \equiv A_2(\mu_d). \tag{A2}$$

1. Outer layer CNL

In this layer, the amplitude varies weakly with respect to the slow variable $X = \mu_1 x$. The change of variable $\mathcal{X} = \mu_1\, x - \mu_0$, where $\mu_0 = \mu_A + \epsilon$ leads to seek a solution of

$$\mathcal{X} A - A^3 + A^5 + \mu_1 U_0 A'(\mathcal{X}) = 0, \tag{A3}$$

where prime denotes differentiation with respect to the argument. Since $\mu_0 \ll 1$ and the derivative $A'(\mathcal{X})$ only appears at first order in μ_1, Eq. (A3) is not an ordinary differential equation and its solution is obtained at each order without free parameter:

$$A(\mathcal{X}) = A_0(\mathcal{X}) + \mu_1 A_1(\mathcal{X}), \tag{A4}$$

with

$$A_0(\mathcal{X}) = \left(\frac{1}{2} + \frac{1}{2}\sqrt{1 - 4\mathcal{X}}\right)^{1/2}, \quad A_1(\mathcal{X}) = \frac{U_0}{4A_0^3(\mathcal{X})[1 - 2A_0^2(\mathcal{X})]^2} \tag{A5}$$

The position of CNL is therefore fixed in space and delimited by the upstream boundary x_s where $A(x)$ is maximum and the downstream boundary x_d where $\mu(x_d) = \mu_d(U_0)$. The solution (A4–A5) may be expanded near the CNL boundaries which correspond to the values $\mathcal{X} = -\mu(x_i) + \mu_1(x - x_i)$, $i = s, d$. Note that $\mu(x_s) = \mu_A + \epsilon - \mu_1 x_s$ whereas with $\mu(x_d) = \mu_d$. This leads to the following expansions, which are not totally symmetric due to the definition of the CNL boundaries:

$$\text{when } x \to x_s\text{: } A(\mathcal{X}) \simeq A_0(-\mu_A) + (\mu_1\, x - \epsilon)A_0'(-\mu_A) + \mu_1 A_1(-\mu_A), \tag{A6}$$

$$\text{when } x \to x_d\text{: } A(\mathcal{X}) \simeq A_0(-\mu_d) + \mu_1\,(x - x_d)A_0'(-\mu_d) + \mu_1 A_1(-\mu_d). \tag{A7}$$

2. Transition layers TL^s and TL^d

In these two layers, the analysis is similar since we seek a solution of Eq. (13) linearized around one of the boundary x_i of CNL, which represents also the center of the layer TL^i ($i = s, d$), and where the amplitude is close to a finite value A_i [see Eqs. (A1,A2)]. We therefore introduce $A = A_i - \epsilon^{p_i}\phi_i(x)$ into Eq. (13) and expand the latter at first order in ϵ^{p_i}. We obtain the equation satisfied by $\phi_i(x)$:

$$\frac{d^2\phi_i}{dx^2} - U_0\,\frac{d\phi_i}{dx} + \tilde{\mu}_i\,\phi_i = \epsilon^{-p_i}A_i\psi_i(x), \tag{A8}$$

where the quantity $\psi_i(x)$ on the right hand side reads as:

$$\psi_s(x) = (\epsilon - \mu_1 x), \qquad \psi_d(x) = -\mu_1(x - x_d) \tag{A9}$$

and $\tilde{\mu}_i = \mu_i + 3A_i^2 - 5A_i^4$, with the convention $\mu_s \equiv \mu_A$. Using the notations

$$k_s^- = -\frac{U_0 + \sqrt{3}}{2}, \quad k_s^+ = \frac{3U_0 + \sqrt{3}}{2}, \quad k_d^- = \frac{3U_0 - \sqrt{3}}{2}, \quad k_d^+ = \frac{-U_0 + \sqrt{3}}{2}, \tag{A10}$$

the general solution of Eq. (A8) then reads as:

$$\phi_i(x) = c_{1i}\mathrm{e}^{k_i^+(x-x_i)} + c_{2i}\mathrm{e}^{k_i^-(x-x_i)} + \epsilon^{-p_i}\frac{A_i}{\tilde{\mu}_i}\psi_i(x) - \mu_1\epsilon^{-p_i}\frac{U_0A_i}{\tilde{\mu}_i^2}, \tag{A11}$$

where the last non-exponential term represents a particular solution of Eq. (A8) and c_{1i}, c_{2i} are integration constants. In each transition layer TL^s and TL^d, one boundary condition will be imposed by the matching with the solution in CNL when $x - x_s \to +\infty$, and when $x - x_d \to -\infty$. The outer solution (A6) in CNL is linear with respect to x; then $\epsilon^{p_s}\phi_s(x)$ and $\epsilon^{p_d}\phi_d(x)$ must be also linear when $x - x_s \to +\infty$ and $x - x_d \to -\infty$, respectively. These two matching conditions imply $c_{1s} = 0$ and $c_{2d} = 0$. When $x - x_s \to +\infty$, or $x - x_d \to -\infty$, the inner solution (A11) admits the expansion

$$\epsilon^{p_i}\phi_i(x) \simeq \frac{A_i}{\tilde{\mu}_i}\psi_i(x) - \mu_1\epsilon^{-p_i}\frac{U_0A_i}{\tilde{\mu}_i^2}. \tag{A12}$$

Since $A_0(-\mu_i) = A_i$, $A_i/\tilde{\mu}_i = A_0'(-\mu_i)$ and $U_0A_i/\tilde{\mu}_i^2 = A_1(-\mu_i)$, expansion (A12) with $i = s$, [$i = d$] represents exactly orders ϵ and μ_1 of the solution (A6) [the solution (A7)], respectively. Hence, matching between CNL and TL^i is done. The quantities c_{1d} and c_{2s} must still be determined.

The position x_s of the maximum amplitude x_s must satisfy $d\phi_s/dx(x_s) = 0$. This condition determines the constant $c_{2s} = \mu_1 \epsilon^{-p_s} A_s/\tilde{\mu}_s k_s^-$. The quantity x_d is defined by $\mu(x_d) = \mu_d$ and hence, $A(x_d) = A_d$ yields the condition $\phi_d(x_d) = 0$, which determines the constant $c_{1d} = \mu_1 \epsilon^{-p_d} A_d U_0/\tilde{\mu}_d^2$. The complete solution (A11) with $i = s$ [$i = d$] are known and in order to match it with the front solution in NF^s [NF^d], we determine its asymptotic behavior when $x - x_s \to -\infty$ [$x - x_d \to +\infty$], respectively, (given by the exponential terms at leading order). Since the matching of these parts of solution will be done in the phase space, we differentiate Eq. (A11) and combine the result with Eq. (A11) again to eliminate the exponential term which appears in the differentiated equation:

$$\epsilon^{p_s} \frac{d\phi_s}{dx} = k_s^- \epsilon^{p_s} \phi_s + \mu_1 x_s \frac{k_s^- A_s}{\tilde{\mu}_s} - \epsilon \frac{k_s^- A_s}{\tilde{\mu}_s} + \mu_1 \frac{A_s}{\tilde{\mu}_s} \left(\frac{U_0 k_s^-}{\tilde{\mu}_s} - 1 \right), \tag{A13}$$

$$\epsilon^{p_d} \frac{d\phi_d}{dx} \simeq k_d^+ \epsilon^{p_d} \phi_d. \tag{A14}$$

Equation (A13) is an exact relation and will be used as the asymptotic behavior of the solution (A11) in the phase space as $x - x_s \to -\infty$, whereas (A14) is truncated at leading order which is sufficient to do the matching when $x - x_d \to +\infty$.

Moreover, the maximum amplitude reads as $A(x_s) = A_s - \epsilon^{p_s} \phi(x_s)$ with

$$\epsilon^{p_s} \phi(x_s) = -\mu_1 \frac{A_s}{\tilde{\mu}_s} x_s + \epsilon \frac{A_s}{\tilde{\mu}_s} + \mu_1 \frac{A_s}{\tilde{\mu}_s} \left(\frac{1}{k_s^-} - \frac{U_0}{\tilde{\mu}_s} \right). \tag{A15}$$

3. Central nonlinear layer NF^s and NF^d

In the front layer layer NF^s [NF^d] which possesses one boundary at x_s, [x_d], we consider that the solution grows [decreases] sufficiently fast so that $\mu(x)$ is approximately constant and equal to μ_s [μ_d]. In other words, the size of the two front layers is much smaller than μ_1^{-1}. The solution in NF^s [NF^d] is then nearly the same as in the homogeneous problem that has been already solved [17]. Indeed, at leading order, the solution in NF^s represents an heteroclinic trajectory in the phase space $(A, dA/dx)$, linking the origin to the point $(A_s, dA/dx = 0)$ for the constant parameter value $\mu = \mu_A$, whereas in NF^d, the solution represents an heteroclinic trajectory linking the point $(A_d, dA/dx = 0)$ to the origin. At the next order, small corrections have to be added, due to the small variation of $\mu(x)$ over the size of NF^s [NF^s].

We therefore seek these solutions directly in the phase space in the form of Eq. (A16):

$$u(A) = \frac{dA}{dx} = u_0(A) + \epsilon\, u_1(A) + \mu_1 u_2(A). \tag{A16}$$

At the lowest order, $u_0(A)$ satisfies

$$u_0 u_0' - U_0 u_0 + \mu_i A + A^3 - A^5 = 0 \tag{A17}$$

where $i = s$ or $i = d$ and a prime denotes differentiation with respect to A. For the value of the parameter μ_i previously defined and an advection velocity $U_0 < 1/\sqrt{3}$, both solutions $u_0(A)$ in NF^s and NF^d are polynomial. When $1/\sqrt{3} < U_0 < \sqrt{3}$, $u_0(A)$ is still polynomial in NF^s but not in NF^d. Since the trailing edge of the NG mode in NF^d and OL is slave of its spatial structure upstream, we present here only the case $U_0 < 1/\sqrt{3}$ without loss of generality. For each layer NF^i, the solution at leading order then reads

$$u_0(A) = \pm\frac{1}{\sqrt{3}} A \left(A_i^2 - A^2\right), \tag{A18}$$

with the plus sign if $i = s$ and the minus sign if $i = d$. This solution may be again integrated:

$$A = A_i \left(1 + A_{0i}^{-2} \mathrm{e}^{-(\pm A_i^2/\sqrt{3})x}\right)^{-1/2} \tag{A19}$$

where A_{0i} is an integration constant.

When $x \to x_i$, the asymptotic behavior of the solution reads as:

$$A = A_i - \frac{A_i}{2A_{0i}^2} \mathrm{e}^{-(\pm 2A_i^2/\sqrt{3})x} \tag{A20}$$

Since $k_s^- = -2A_s^2/\sqrt{3}$ [$k_d^+ = 2A_d^2/\sqrt{3}$], the solution (A20) with the plus [minus] sign matches with the solution (A11) in TL^s [TL^d], respectively. This determines the constants

$$A_{0s}^{-2} = \frac{2\mu_1}{\tilde{\mu}_s k_s^-} \mathrm{e}^{-k_s^- x_s} \quad \text{and} \quad A_{0d}^{-2} = \frac{2\mu_1 U_0}{\tilde{\mu}_d^2} \mathrm{e}^{-k_d^+ x_d}. \tag{A21}$$

By reporting these values in Eq. (A19), we find the asymptotic behavior of the solution in TL^d when $x - x_d \to +\infty$:

$$A \simeq A_d \frac{\tilde{\mu}_d}{\sqrt{2U_0\mu_1}} \mathrm{e}^{-k_d^+(x-x_d)/2} \tag{A22}$$

In NF^d, this leading order is sufficient to do the matching with OL as will be seen below, but in NF^s, we have to compute the correction to the leading order. This next order to be taken into account may be either ϵ or $\mu_1 x$; We assume that they are separated; $u_1(A)$ and $u_2(x, A)$ satisfy

$$u_0\, u_1' + (u_0' - U_0)\, u_1 = -A \tag{A23}$$

$$u_0\, u_2' + (u_0' - U_0)\; u_2 = x\, A \tag{A24}$$

where x in (A24) is at first order the function of A defined by Eq. (A19), with the corresponding constant A_{0s}, which reads

$$x(A) = x_s - \frac{1}{k_s^-}\left[\log\left(\frac{A^2}{A_s^2 - A^2}\right) - \log\left(\frac{\tilde{\mu}_s k_s^-}{2\mu_1}\right)\right] \tag{A25}$$

Since $u_0(A)$ is a polynomial solution, u_1 and u_2 can be obtained analytically by introduction of Eq. (A18) in Eqs. (A23,A24) and of Eq. (A25) in Eq. (A24). By integration of the resulting equations, we obtain

$$u_1(A) = -\sqrt{3} A^{\lambda_1} (A_s^2 - A^2)^{\lambda_2} \int_{A_s}^{A} a^{-\lambda_1} (A_s^2 - a^2)^{-\lambda_2 - 1} da \tag{A26}$$

where

$$\lambda_1 = \frac{3U_0 - \sqrt{3}}{U_0 + \sqrt{3}}, \qquad \lambda_2 = -\frac{3U_0 + \sqrt{3}}{U_0 + \sqrt{3}}, \tag{A27}$$

and

$$u_2(A) = \sqrt{3} A^{\lambda_1} (A_s^2 - A^2)^{\lambda_2} \int_{A_s}^{A} a^{-\lambda_1} (A_s^2 - a^2)^{-\lambda_2 - 1} x(a) da \tag{A28}$$

where $x(a)$ is the function of a defined by Eq. (A25).

When $A \to A_s$, the solution (A16) may be expanded as

$$u_0(A) + \epsilon u_1(A) + \mu_1 u_2(A) \simeq -\frac{2A_s^2}{\sqrt{3}}(A_s - A) - \epsilon \frac{\sqrt{3}}{2A_s\lambda_2} + \mu_1 \frac{\sqrt{3}}{2A_s\lambda_2}\left(x - \frac{\sqrt{3}}{2A_s^2\lambda_2}\right) \tag{A29}$$

which is identical to expansion (A13) since we verify that $k_s^- = -2A_s^2/\sqrt{3}$, $k_s^- A_s/\tilde{\mu}_s = \sqrt{3}/2A_s\lambda_2$ and $(A_s/\tilde{\mu}_s)(U_0 k_s^-/\mu_s - 1) = -3/4A_s^3\lambda_2^2$. The solutions in TL^s and NF^s are now matched. In other words, the matching succeeds whatever the size of the transition layer TL^s. When $A \to 0$, the solution $u(A)$ defined by Eqs. (A16,A18,A26,A28) admits the expansion

$$u_0(A) + \epsilon u_1(A) + \mu_1 u_2(A) \simeq \frac{A_s^2}{\sqrt{3}} A + \sqrt{3} A^{\lambda_1} A_s^{2\lambda_2} \times \\ \left\{ B[\epsilon - \mu_1(x_s - \frac{1}{k_s^-}\log\mu_1) - \frac{\mu_1}{k_s^-}\log\frac{\tilde{\mu}_s k_s^-}{2}] + \mu_1 \frac{\sqrt{3}}{A_s^2}\Gamma \right\} \tag{A30}$$

where

$$B = \int_0^{A_s} a^{-\lambda_1}(A_s^2 - a^2)^{-\lambda_2 - 1} da, \quad \Gamma = \int_0^{A_s} a^{-\lambda_1}(A_s^2 - a^2)^{-\lambda_2 - 1} \log \frac{a}{\sqrt{A_s^2 - a^2}} da.$$

4. Transition layer IL

In this layer, the amplitude is small since A vanishes at $x = 0$. Denoting ξ the inner variable which is connected to the amplitude by the relation $A = \theta(\epsilon)\xi$ (where $\theta(\epsilon)$ denotes the size in amplitude of the inner layer and will be precised by the matching), ξ satisfies the linearized Eq. (13) around $A = 0$:

$$\xi'' - U_0\, \xi' + \mu(x)\xi = 0. \qquad \text{(A31)}$$

Since $\xi(x)$ must vanish at the origin, the solution of Eq. (A31) may be written with one undetermined integration constant v_0, and using Airy functions [42]

$$\xi(x) = \frac{v_0 \pi}{\mu_1^{1/3}} \mathrm{e}^{U_0 x/2} \left\{ a \,\mathrm{Bi}\left[(x - x_K)\mu_1^{1/3}\right] - b \,\mathrm{Ai}\left[(x - x_K)\mu_1^{1/3}\right] \right\} \qquad \text{(A32)}$$

where $x_K = (\mu_A - U_0^2/4 + \epsilon)/\mu_1$ is the position at which $\mu(x)$ reaches $U_0^2/4$ (x_K is negative since $\mu_A(U_0) < U_0^2/4$), $a = \mathrm{Ai}(-x_K \mu_1^{1/3})$ and $b = \mathrm{Bi}(-x_K \mu_1^{1/3})$. The slope v_0 at the origin of the inner solution (A32) will be fixed by the matching. Since $\mu_1 \ll 1$, we obtain $-x_K \mu_1^{1/3} \gg 1$. Hence, the Ai and Bi functions may be replaced by their asymptotic expansions at infinity. The same inner solution than for homogeneous NG mode [17] is found and read as:

$$\xi(x) = \frac{v_0}{r^+ - r^-} \left(\mathrm{e}^{r^+ x} - \mathrm{e}^{r^- x} \right) \qquad \text{(A33)}$$

where $r^+ = (U_0 + \sqrt{3})/4$ and $r^- = (3U_0 - \sqrt{3})/4$.

5. outer layer OL

In the outer layer OL, $A(x)$ is small since it must vanish at infinity. Therefore, $A(x)$ is solution of the linear equation (A31) and reads

$$A(x) = g(\mu_1) \mathrm{e}^{\frac{U_0}{2} x} \,\mathrm{Ai}\left[(x - x_K){\mu_1}^{\frac{1}{3}}\right] \qquad \text{(A34)}$$

where $g(\mu_1)$ is an integration constant (the coefficient of Bi must be zero in order to cancel the growing part of the general solution).

In order match the solutions in OL and NF^d, let us expand (A34) when $x \to x_d$. Since $x - x_K = x_d - x_K + x - x_d$, and $x_d - x_K \sim (U_0 + \sqrt{3})^2/16\mu_1$, $x_d \sim (\mu_A - \mu_d)/\mu_1 = \sqrt{3}U_0/4\mu_1$, we may use the asymptotic behavior of Ai at infinity [42] to find

$$A(x) \simeq g(\mu_1)\mu_1^{1/6} \frac{\mathrm{e}^{[12\sqrt{3}U_0^2 - (U_0+\sqrt{3})^3]/96\mu_1}}{[\pi(U_0 + \sqrt{3})]^{1/2}} \mathrm{e}^{-k_d^+(x-x_d)/2} \tag{A35}$$

where we have used $-k_d^+/2 = U_0/2 - [\mu_1(x_d - x_K)]^{1/2}$. Equation (A35) must be identified with Eq. (A22) and therefore

$$g(\mu_1) = \frac{3}{16}\left(\frac{3\pi}{2}\right)^{1/2} \mu_1^{-2/3} \mathrm{e}^{[(U_0+\sqrt{3})^3 - 12\sqrt{3}U_0^2]/96\mu_1} \times \left(1 + \frac{\sqrt{3}}{U_0}\right)^{1/2} \left(U_0 - \frac{1}{\sqrt{3}}\right)(U_0 - \sqrt{3})^2. \tag{A36}$$

REFERENCES

[1] P. Huerre and P. A. Monkewitz, Local and global instabilities in spatially developing flows, Ann. Rev. Fluid. Mech. **22**, 473–537 (1990).

[2] M. Taki, N. Ouarzazi, H. Ward, P. Glorieux, Nonlinear front propagation in optical parametric oscillators, J. Opt. Soc. Am. B **17**, 997 (2000).

[3] P. Gondret, P. Ern, L. Meignin and M. Rabaud, Experimental evidence of a nonlinear transition from convective to absolute instability, Phys. Rev. Lett. **82**, 1442-1445 (1999).

[4] H. W. Müller, M. Lücke, and M. Kamps, Transversal convection patterns in horizontal shear flow, Phys. Rev. A **45**, 3714–3726 (1992). H. W. Müller, M. Lücke, and M. Kamps, Convective patterns in horizontal flow, Europhys. Lett. **10**, 451–456 (1989).

[5] P. Büchel, M. Lücke, D. Roth, and R. Schmitz, Pattern selection in the absolutely unstable regime as a nonlinear eigenvalue problem: Taylor vortices in axial flow, Phys. Rev. E **53**, 4764–4777 (1996).

[6] A. Couairon and J.-M. Chomaz, Pattern selection in the presence of a cross flow, Phys. Rev. Lett. **79**, 2666–2669 (1997).

[7] A. Couairon and J.-M. Chomaz. Primary and secondary nonlinear global instability. *Physica D*, **132**, 428–456 (1999).

[8] S. M. Tobias, M. R. E. Proctor and E. Knobloch, Convective and absolute instabilities of fluid flows in finite geometry, Physica D **113**, 43–72 (1998). Ibid, The role of absolute instability in the solar dynamo, Astron. Astrophys. **318**, L55–L58 (1997).

[9] A. Couairon and J.-M. Chomaz, Fully nonlinear global modes in slowly varying flows, Phys. Fluids. **11**, 3688–3703 (1999).

[10] B. Pier, P. Huerre, J.-M. Chomaz and A. Couairon, Steep nonlinear global modes in spatially developing media, Phys. Fluids. **10**, 2433-2435 (1998). B. Pier, P. Huerre and J.-M. Chomaz. Physica D **148**, 49 (2001).

[11] A. P. Bassom, K. M. Kuzanyan, A. M. Soward, A nonlinear dynamo wave riding on a

spatially varying background, Proc. R. Soc. Lond. A **455**, 1443-1481 (1999).

[12] A. M. Soward, Thin aspect ratio $\alpha\omega$-dynamos in galactic discs and stellar shells, in Advances in nonlinear dynamos, (eds. M. Núñez and A. F. Mas), to appear.

[13] R. J. Briggs. Electron-Stream Interaction with Plasmas. MIT Press, Cambridge, MA, 1964.

[14] A. Bers. Space time evolution of plasma instabilities – absolute and convective, In M. N. Rosenbluth and R. Z. Sagdeev, editors, Handbook of Plasma Physics, pages 451–517, Amsterdam, 1983. North-Holland.

[15] E. M. Lifshitz and L. P. Pitaevskii, Physical kinetics, Pergamon, London, 1981.

[16] A. Couairon and J.-M. Chomaz, Global instability in nonlinear systems, Phys. Rev. Lett. **77**, 4015–4018 (1996).

[17] A. Couairon and J.-M. Chomaz, Absolute and convective instabilities, front velocities and global modes in nonlinear systems, Physica D **108**, 236–276 (1997).

[18] G. Ahlers and D. S. Cannel, Vortex-front propagation in rotating Couette–Taylor flow, Phys. Rev. Lett **50**, 1583 (1983).

[19] J. Fineberg and V. Steinberg, Vortex-front propagation in Rayleigh–Bénard convection, Phys. Rev. Lett **58**, 1332 (1987).

[20] A. Hanna, A. Saul and K. Showalter, Detailed studies of propagating fronts in the iodate oxydation of arsenous acid, J. Am. Chem. Soc. **104**, 3838 (1982).

[21] A. Kolmogorov, I. Petrovsky and N. Piskunov, Investigation of a diffusion equation connected to the growth of materials, and application to a problem in biology, *Bull. Univ. Moscow, Ser. Int. Sec. A* **1**, 1 (1937).

[22] A. C. Newell, T. Passot and J. Lega, Order parameter equations for patterns, Annu. Rev. Fluid Mech. **25**, 399 (1993).

[23] D. G. Aronson and H. F. Weinberger, Multidimensional nonlinear diffusion arising in population genetics, Adv. Math. **30**, 33 (1978).

[24] M. Bramson, Mem. Am. Math. Soc. bf 285, 1 (1983).

[25] W. van Saarloos, Dynamical velocity selection: marginal stability, Phys. Rev. Lett. **58**, 2571 (1987). *Ibid.*, Front propagation into unstable states: marginal stability as a dynamical mechanism for velocity selection, Phys. Rev A **37**, 211 (1988). *Ibid.*, Front propagation into unstable states: II Linear versus nonlinear marginal stability and rate of convergence, Phys. Rev A **39**, 6367 (1989). W. van Saarloos and P. C. Hohenberg, Pulses and fronts in the complex Ginzburg–Landau equation near a subcritical bifurcation, Phys. Rev. Lett. **64**, 749 (1990).

[26] W. van Saarloos and P. C. Hohenberg, Fronts, pulses, sources and sinks in generalized complex Ginzburg–Landau equations, Physica D **56**, 303 (1992).

[27] E. Ben-Jacob, H. R. Brand, G. Dee, L. Kramer and J. S. Langer, Pattern propagation in nonlinear dissipative systems, Physica D **14**, 348 (1985). G. Dee, Dynamical properties of propagating front solutions of the amplitude equations, Physica D **15**, 295 (1985). *Ibid.*, Propagation into an unstable state, J. Stat. Phys. **39**, 705 (1985). G. Dee and J. S. Langer, Phys. Rev. Lett. **50**, 749 (1990).

[28] J. A. Powell, A. C. Newell and C. K. R. T. Jones, Competition between generic and nongeneric fronts in envelope equations, Phys Rev. A **44**, 3636 (1991).

[29] G. C. Paquette and Y. Oono, Structural stability and selection of propagating fronts in semilinear parabolic partial differential equations, Phys. Rev. E **49**, 2368 (1994).

[30] R. D. Benguria and M. C. Depassier, Speed of fronts of the reaction-diffusion equation, Phys. Rev. Lett. **77**, 1171 (1996).

[31] E. Brunet and B. Derrida, Shift in the velocity of a front due to a cutoff, Phys. Rev. E **56**, 2597 (1997).

[32] U. Ebert and W. van Saarloos, Universal algebraic relaxation of fronts propagating into an unstable state and implications for moving boundary approximations, Phys. Rev. Lett. **80**, 1650 (1998).

[33] J.-M. Chomaz and A. Couairon, Propagating pattern selection and causality reconsid-

ered, Phys. Rev. Lett. **84**, 1910–1914 (2000).

[34] B. J. A. Zielinska and J. E. Wesfreid, On the spatial structure of global modes in wake flow, Phys. Fluids **7**, 1418–1424 (1995).

[35] S. Goujon-Durand, P. Jenffer, and J. E. Wesfreid, Downstream evolution of the Bénard-von Kármán instability. Phys. Rev. E **50**, 308 (1994).

[36] H. Ward, M. N. Ouarzazi, M. Taki, P. Glorieux, Transverse dynamics of optical parametric oscillators in presence of walk-off. Eur. Phys. J. D **3**, 275–288 (1998). H. Ward, M. N. Ouarzazi, M. Taki, P. Glorieux, Influence of walk-off on pattern formations in non-degenerate optical parametric oscillators, Phys. Rev. E **63**, 013701 (2001).

[37] N. Meunier, M. R. E. Proctor, D. Sokoloff, A. M. Soward and S. M. Tobias, Asymptotic properties of a nonlinear $\alpha\omega$-dynamo wave: Period, amplitude and latitude dependence, Geophys. Astrophys. Fluid Dynam. **86**, 249-285 (1997).

[38] J.-M. Chomaz, P. Huerre, and L. G. Redekopp, Bifurcations to local and global modes in spatially developing flows, Phys. Rev. Lett. **60**, 25–28 (1988).

[39] J.-M. Chomaz and A. Couairon, Against the wind, Phys. Fluids, **11**, 2977-2983 (1999).

[40] J.-M. Chomaz, Absolute and convective instabilities in nonlinear systems, Phys. Rev. Lett. **69**, 1931–1934 (1992).

[41] C. M. Bender and S. A. Orszag, *Advanced mathematical methods for scientists and engineers*, Mc Graw Hill, 1978.

[42] M. Abramowitz and I. A. Stegun, *Handbook of mathematical functions*, Dover, New York, 1972.

List of captions

Fig. 1: Spatial structure of a homogeneous nonlinear global mode.

Fig. 2: Parameter space of the homogeneous problem. For the sake of clarity, the axis scales are not linear. HNG modes exist in the shaded regions. For $U_0 > \sqrt{3}$, the transition to global instability is of the Kolmogorov (K) type (simultaneous with the transition from convective to absolute instability). For $U_0 < \sqrt{3}$ the transition is of nonlinear type (N), occurring while the basic state is convectively unstable or stable. The fine curve illustrates the K transition and bounds the (dark gray) region of absolute instability. The curve $\mu_d(U_0)$ is discussed in the text.

Fig. 3: A NG mode displays clearly four parts: in the nonlinear front layer NF^s (NF^d), the solution steepens while growing (decreasing). In the central nonlinear layer CNL, the solution decreases softly. OL is an outer linear region where the amplitude is small. An inner layer IL at the origin, and two transition layers (TL^s around the maximum amplitude, TL^d around the end of the weakly varying part of the solution) connect linear and nonlinear regions. The solid line represents the bifurcation parameter $\mu(x)$.

Fig. 4: The solution shown in Fig. 3 is plotted in the phase space $(A, x, dA/dx)$. The solution in NF^s and NF^d lay nearly in planes $(A, dA/dx)$, whereas in CNL, it lays nearly in the plane (A, x).

Fig. 5: (a) Envelope $|A|$ and real part $\mathrm{Re}(A)$ of pushed global modes with pushed front stopped by the boundary $x = 0$ and sharp tail in the form of a decreasing front. (b) Same as in (a) but a saddle node bifurcation induces the return to zero in the tail. (c) Envelope $|A|$ and real part $\mathrm{Re}(A)$ of pushed global modes with disordered behavior in the tail as the saturated traveling wave becomes unstable when x varies. (d) variation of the parameters used in (c). (e) Example of solution in parameters region where a pushed mode is not selected.

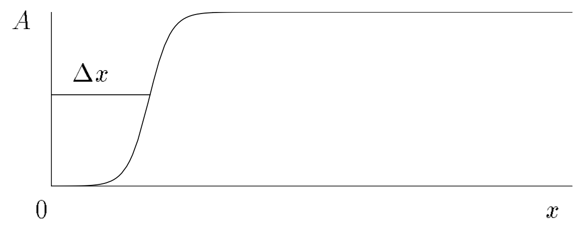

FIG. 1. Spatial structure of a homogeneous nonlinear global mode.

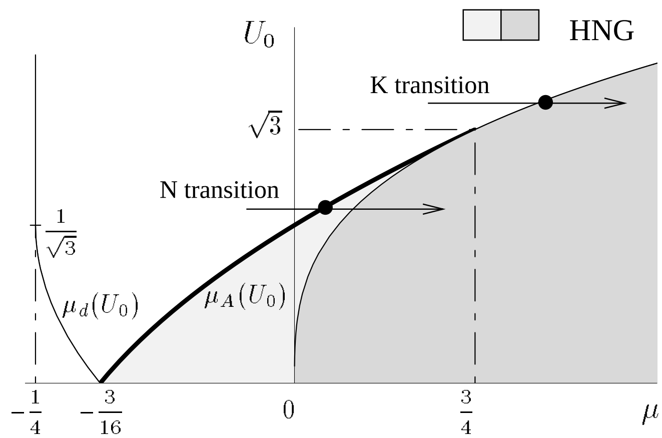

FIG. 2. Parameter space of the homogeneous problem. For the sake of clarity, the axis scales are not linear. HNG modes exist in the shaded regions. For $U_0 > \sqrt{3}$, the transition to global instability is of the Kolmogorov (K) type (simultaneous with the transition from convective to absolute instability). For $U_0 < \sqrt{3}$ the transition is of nonlinear type (N), occurring while the basic state is convectively unstable or stable. The fine curve illustrates the K transition and bounds the (dark gray) region of absolute instability. The curve $\mu_d(U_0)$ is discussed in the text.

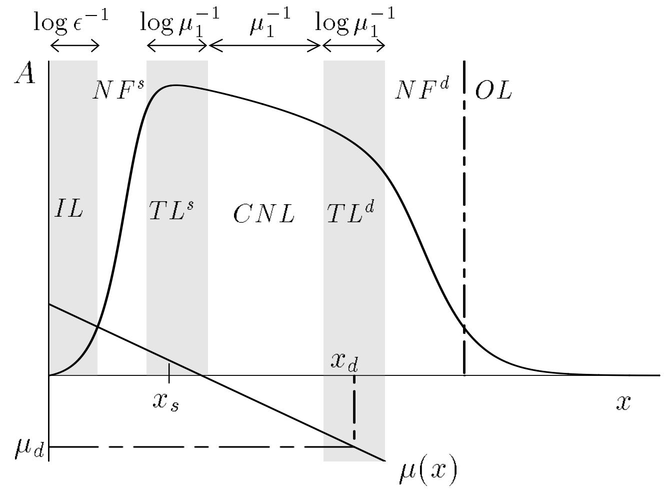

FIG. 3. A NG mode displays clearly four parts: in the nonlinear front layer NF^s (NF^d), the solution steepens while growing (decreasing). In the central nonlinear layer CNL, the solution decreases softly. OL is an outer linear region where the amplitude is small. An inner layer IL at the origin, and two transition layers (TL^s around the maximum amplitude, TL^d around the end of the weakly varying part of the solution) connect linear and nonlinear regions. The solid line represents the bifurcation parameter $\mu(x)$.

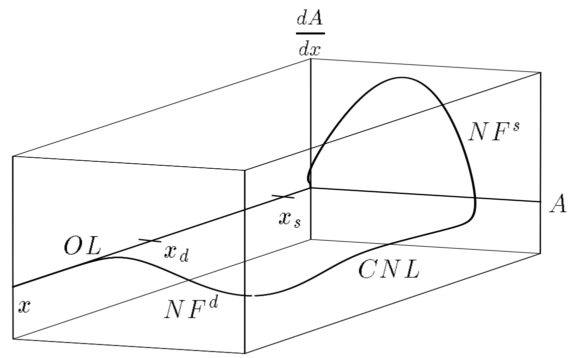

FIG. 4. The solution shown in Fig. 3 is plotted in the phase space $(A, x, dA/dx)$. The solution in NF^s and NF^d lay nearly in planes $(A, dA/dx)$, whereas in CNL, it lays nearly in the plane (A, x).

FIG. 5.